13th ewtec 2019 Proceedings of the 13th European Wave and Tidal Energy Conference 1-6 Sept 2019, Naples, Italy

"Far Field" effects of arrays of wave energy converters in irregular long–crested and short-crested waves: a comparative study

Gael Verao Fernandez, Philip Balitsky, Panagiotis Vasarmidis, Nicolas Quartier, Vasiliki Stratigaki and Peter Troch

***Abstract*—The objective of this paper is to compare the difference between the "far field" effects of different WEC(s) types: a heaving cylindrical wave energy converter (HCWEC) and an oscillating surge wave energy converter (OSWEC) in unidirectional long-crested waves and short-crested waves. A recently developed coupling methodology between the wave propagation model MILDwave and the wave-structure interaction solver NEMOH is used. The difference in the "far field" effects will be accounted in terms of the disturbance coefficient K_D. The results of the HCWEC and the OSWEC are compared for 1 WEC and a 5 WEC array in terms of difference in K_D between long crested and short crested waves. For 1 WEC the difference between long crested and short crested waves is negligible. In contrast, for the 5 WEC array the K_D in short crested waves in the lee of the array is reduced a 3% and a 7% for the HCWEC and OSWEC, respectively. Consequently, we can observe that to avoid overestimating the impact of WEC arrays it is necessary to simulate WEC interaction under short crested waves sea states.**

***Index Terms*—numerical coupling; MILDwave; NEMOH;far field;wave energy converter arrays;short crested waves; periodic lateral boundaries**

I. Introduction

OCEAN waves are a vast resource of marine renewable energy that has the potential to contribute reducing the world's dependency on fossil fuels. In the recent years, a large number of Wave Energy Converters (WECs) have been under development with none of them yet reaching commercial stage [1]. Nonetheless, WECs will have to be deployed in large numbers with a closely spaced configuration, commonly known in literature as WEC arrays, in order to be economically viable. Due to the hydrodynamics interactions between the WECs of an array the surrounding wave field will be affected, both close to the WECs ("near field" effects) and in the coastal zone ("far field" effects). Substantial research has been carried out to study the "near field" effects focusing on optimizing the array configuration to maximize power output using wave structure interaction solvers. Far field effects have also been studied using wave propagation models to identify the location of "hot spots" (increased wave height regions) and "wake zones" (reduced wave height regions) due to the presence of the WEC array. In the recent years, coupling methodologies between wave-structure interaction solvers and wave propagation models have been developed to combine the strengths of both types of models and obtain a better understanding of the "near field" and "far field" effects.

Typically, studies with those three numerical approaches (wave-structure interaction solvers to calculate the "near field" effects, wave structure interaction solvers to calculate the "far field" effects and coupling models to calculate both "near" and "far-field" effects) are carried out using unidirectional irregular long-crested waves. Nevertheless, real ocean waves have a directional spreading since they do not propagate in a single direction. These waves are referred in literature as short crested waves. As pointed out in [2] the performance of WEC arrays changes in short-crested sea states. A change in the performance of the WEC array will then have an impact in the "far field" effects.

In the present investigation, the one-way coupling methodology presented in [3] is employed to compare the "wake effects" of WEC arrays under long and short crested irregular wave conditions. Two type of WEC with different absorption principles have been chosen and tested individually and for a 5 WEC array configuration. The structure of the paper is as follows: Section I provides a short overview of the state-of-the-art and problem statement. Section II provides a description of the coupling methodology and the numerical set-up employed for the simulations. Section III presents the results and the discussion of the different Test Cases. Finally the conclusions and further work are drawn in Section IV

II. Numerical Framework

A. Coupling methodology

The numerical modelling in this research is performed using a recently developed and validated coupled model between the wave propagation model MILDwave and the wave-structure interaction solver NEMOH [3]–[5]. This coupled model allows to obtain the total wave field around a WEC array as a superposition of the incident, radiated and diffracted wave fields. It can be described as a one-way coupled model where the two numerical models simulations

1651-WHM

All the authors are with the Department of Civil Engineering, Ghent University, Technologiepark 60, B-9052 Zwijnaarde, e-mail: gael.veraofernandez@ugent.be, philip.balitsky@ugent.be, panagiotis.vasarmidis@ugent.be, nicolas.quartier@ugent.be, vasiliki.stratigaki@ugent.be, peter.troch@ugent.be

 Copyright © European Tidal and Wave Energy Conference 2019

are performed independently and it consists of four steps:

1) A first simulation is performed in MILDwave to obtain the incident wave field in the time-domain, without any floating structure in the numerical basin. The wave characteristics at the coupling location are computed and used as input values for NEMOH.
2) A second simulation is performed in NEMOH to calculate the perturbed wave field around the floating structure at the coupling location in the frequency-domain.
3) A third simulation is performed in MILDwave to obtain the perturbed wave field in the time-domain. The perturbed wave field from NEMOH is transformed from the frequency-domain to the time-domain and coupled into MILDwave by prescribing an internal wave generation boundary.
4) Finally, the total wave field is obtained as the combination of the incident and perturbed wave fields calculated in MILDwave in the time-domain.

The basis for the coupling methodology employed can be found in [4], [6], [7] and the fundamentals of the MILDwave-NEMOH coupled model have been reported in [3], [5]. The superposition of diffracted and radiated wave field will be referred as the perturbed wave field.

B. The wave propagation model, MILDwave

MILDwave is a mild-slope wave propagation model based on the depth-integrated equations of Radder and Dingemans [8], developed at the Coastal Engineering Research Group of Ghent University, Belgium. MILDwave allows to solve shoaling and refraction of waves propagating over mild slope varying bathymetries under regular, irregular long crested and irregular short crested wave conditions. In the past years, it has been widely used to study wave penetration inside harbours [9] and "far field" effects of WEC arrays [4], [6], [10]–[15].

The mild-slope equations (Equations 1 and 2) are resolved using a finite difference scheme that consists of a two-step space-centered, time-staggered computational grid, as detailed in [16].

$$\frac{\partial \eta}{\partial t} = \frac{\omega^2 - k^2 C C_g}{g}\varphi - \nabla\left(\frac{C C_g}{g}\nabla\varphi\right), \tag{1}$$

$$\frac{\partial \varphi}{\partial t} = -g\eta, \tag{2}$$

where η and φ are, respectively, the free water surface elevation and the wave velocity potential at the free water surface, g is the gravitational acceleration, C is the phase velocity and C_g is the group velocity for a wave with wave number k and angular frequency ω.

MILDwave uses an internal wave generation as introduced by Lee [17]. In addition, by applying the superposition principle, a first order irregular wave is represented as the finite sum of N regular wave components characterized by their wave amplitude, a_j, and wave period, T_j, derived from the wave spectral density, S_j:

$$\eta_{irr}(x,y,t) = \sum_{j=1}^{N} a_j \cos(\omega_j t - k_j(x\cos\theta_j + y\sin\theta_j) + \varphi_j), \tag{3}$$

where

$$a_j = \sqrt{2S_j(f_j)\cdot\Delta f_j}, \tag{4}$$

here $\eta_{I,irreg}$ is the incident irregular wave surface elevation and a_j is the wave amplitude, ω_j is the wave angular frequency, f_j is the wave frequency, k_j is the wave number, θ_j is the wave direction and φ_j is the incident phase, of each wave frequency component. φ_j is selected randomly between $-\pi$ and π to avoid local attenuation of η_{irr}.

In order to generate a short crested wave field the Sand and Mynett method [18] in combination with periodic boundaries has been applied. Figure 1 shows a schematic of the MILDwave wave generation using a single wave generation line parallel to the y-axis combined with the periodic lateral boundaries implementation. At the position of the periodic boundaries, Equations 1 and 2 are solved as if the horizontal boundaries were next to each other. A detailed description of the implementation in MILDwave can be found in [19].

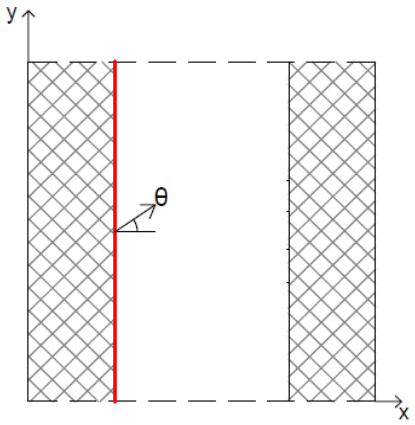

Fig. 1. MILDwave wave generation technique by [19] employed in the MILDwave-NEMOH coupled model. The internal wave generation line is marked using a red line. The period lateral boundaries are indicated by black dashed lines. Figure adapted from [19].

C. The wave-structure interaction solver NEMOH

NEMOH is an open source potential flow BEM solver, developed at Ecole Central de Nantes [20]. It is based on linear potential flow theory [21] and the description of the fundamental equations are reported in [20]. NEMOH is used to solve the diffraction/radiation problem within linear theory, and it has been utilized in a long range of investigations regarding WEC array control and optimization, for example [12], [22], [23].

NEMOH solves the Laplace Equation (5) for the complex wave velocity potential, Φ:

$$\nabla\Phi = 0. \tag{5}$$

The free surface elevation η is calculated by taking the real part of the complex potential $\overline{\eta}$ from the free surface boundary condition, presented by equation 6. From the superposition principle, free surface elevations can be obtained separately from the vertical motions of the WEC(s) due to the diffracted and radiated potentials.

$$\eta = -\frac{1}{g}\left(\frac{\partial\varphi}{\partial t}\right)_{z=0}, \tag{6}$$

where g is the acceleration of gravity.

D. Irregular wave conditions

A long crested and a short crested irregular sea state will be generated using a significant wave height of $H_s = 2$ m and a peak period of $T_p = 8$ s. The long crested irregular waves will be obtained using a Pierson-Moskovitz (P-M) spectrum in Equations (3) and (4), with a total of N_f frequency components and the wave direction of each component equal to the mean wave propagation ($\theta_j = \theta_{mean}$). The P-M irregular wave spectrum is defined by equation 7:

$$S(f) = \frac{B}{f^5}e^{-\frac{C}{f^4}}, \tag{7}$$

where,

$$B = \frac{5}{16}\frac{H_s^2}{T_p^4}, \tag{8}$$

$$C = \frac{5}{4}\frac{1}{T_p^4}. \tag{9}$$

In the case of short crested waves the $S(f)$ will be obtain using the P-M formulation but the wave directions, θ_j, introduced in Equation (3) will be obtained for each frequency and to synthesize a real sea wave field the Sand and Mynnet method will be applied. According to this method the wave spectrum is discretized in N_f frequency components and the wave propagation angles θ_j are selected at random according to the cumulative distribution function of the directional spreading function $D(f,\theta)$ and are assigned to each frequency component. This model provides an accurate representation of the targeted spreading function shape as shown in [19]. The spreading function of [24] is employed :

$$\begin{aligned} &D(f,\theta) = \frac{1}{\sqrt{\pi}}\frac{\Gamma(s_1+1)}{\Gamma\left(s_1+\frac{1}{2}\right)}\cos^{2s_1}(\theta-\theta_{mean}), \\ &-\frac{\pi}{2} < \theta-\theta_{mean} < \frac{\pi}{2}, \end{aligned} \tag{10}$$

where s_1 is the directional spreading parameter, Γ is the Gamma function and θ_{prop} is the wave propagation angle.

$$\sigma_\theta = \sqrt{2 - \frac{2\Gamma^2(s_1+1)}{\Gamma\left(s_1+\frac{1}{2}\right)\Gamma\left(s_1+\frac{3}{2}\right)}}. \tag{11}$$

Hence, the values of s_1 and σ_θ can be determined for swell waves:

$$s_1 = 15.8 \rightarrow \sigma_\theta = 10°. \tag{12}$$

E. Modelled WECs and array layout

Two different type of WEC(S) are studied in this paper to account for the difference in the total wave field under long crested and short crested irregular wave conditions:

1) Heaving Cylindrical Wave Energy Converter (HCWEC): The first type of WEC investigated in this study is a disc shaped heaving buoy with a diameter of 20 m and a draft of 2 m. These WECs are designed to be deployed in deep water at depths around 30 m. This shape has been selected as it is one of the most investigated WEC types with several prototypes reaching pre-commercial WEC array testing stage [1].
2) Oscillating Wave Surge Energy Converter (OSWEC): The second type of WEC is a bottom-fixed pitching flap driven by surge motion of the waves, also referred as OSWEC. This devices are designed to be deployed in shallow water at depths of 10 - 20 m. Our simulated device has dimensions of 20 m width, 1 m thickness and 12 m height, and it is hinged at the sea base with pitching motion about its bottom end. This shape has been selected as it is together with the HCWEC one of the most investigated WEC types with several prototypes been developed [1] over the past years.

First each WEC is modelled independently over a constant bathymetry with a depth corresponding to the expected deployment site. Secondly the two WEC array layouts included in Figure 2 will be modelled. A staggered configuration has been chosen as it has been used in a wide number of studies and has shown to maximize the total power output of the WEC array thus maximizing its impact on the wave field. [25]–[27]

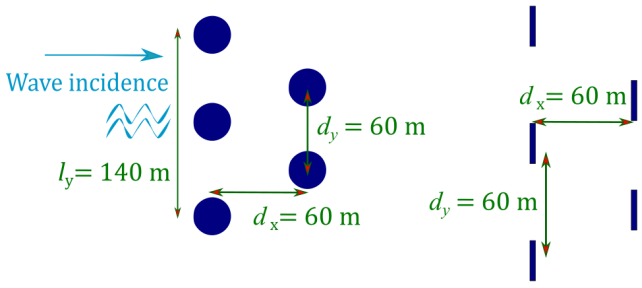

Fig. 2. Plane (TOP) view of the array layout for 5 HCWEC and 5 OSWEC.

F. Test Cases

The objective of this paper is to compare the obtained wave field of a WEC (array) under long and short crested irregular waves. For this matter, a "Test Case" program based on different type of WECs and array configurations, and wave conditions has been designed:

TABLE I
TEST CASES FOR $H_s = 2$ M, $T_p = 8$ S AND $\theta_{mean} = 0^o$

Test Case Number ♯	N_f	s_1	WEC Type	No. WECs	Depth (m)
1	20	0	HCWEC	1	30.0
2	50	15.8	HCWEC	1	30.0
3	20	0	HCWEC	5	30.0
4	20	15.8	HCWEC	5	30.0
5	20	0	OSWEC	1	10.0
6	50	15.8	OSWEC	1	10.0
7	20	0	OSWEC	5	10.0
8	50	15.8	OSWEC	5	10.0

G. Numerical set-up

Following the methodology reported in [3] two numerical wave basins are used in the MILDwave numerical domain: an empty numerical wave basin (ENWB) and a perturbed wave numerical wave basin (RDWB). The effective domain of both numerical basins is set to $L_{x,MW} = L_{y,MW} = 2000$ m. The simulation grid size is chosen to be equal to $\frac{L}{20} = d_x = d_y = 4$ m, while the output gird size is $d_{x,out} = d_{y,out} = 20$ m. The time step employed is $d_t = 0.3$ s providing a sample of 500 waves representative of a developed sea state. The K_d is computed for a simulation time of 4000 s.

For the ENWB, waves are generated using a wave generation line located at the left side of the numerical domain. Two equally sized sponge layers of size $B_{sponge} = 5 \cdot L_{max}$, where L_{max} is the maximum wave length of the discretized incident wave spectrum, are located at the left and right sides of the domain to avoid unwanted reflection at the ends of the basin.

For the RDWB, waves are generated at the center of the domain using a circular wave generation boundary where the perturbed wave wave field calculated in NEMOH is coupled into MILDwave using different wave generation radii equal to the distance from the center of the of the coupling region to the most external WEC plus $0.5 \cdot L_{max}$. Identically, four equally sized sponge layers of size $B_{sponge} = 5 \cdot L_{max}$ are located at the four sides of the domain to avoid unwanted reflection and that the perturbed wave wave propagates through the periodic boundaries.

To obtain the input surface elevation at the circular wave generation line in the RDWB a NEMOH simulation is carried out obtaining the perturbed wave complex surface elevations at the radii of the coupling region. The NEMOH numerical domain is set to $L_{x,NM} = L_{y,NM} = 400$ m providing that it is sufficient to fit the different coupling radii. The HCWEC is descretized using 200 panels, while for OSWEC a total of 300 panels are used. The effect of the PTO has been taken into account calculating the $B_{PTO,opt}$ that maximizes the energy conversion for a single device in regular waves [28] using as input the peak angular frequency, ω_p:

$$B_{PTO,opt} = \sqrt{B_{hyd}^2 + \left(\omega_p(m + M_A) - \frac{K_H}{\omega_p}\right)^2}, \quad (13)$$

where B_{hyd} is the hydrodynamic damping coefficient, m is the WEC mass, M_A is the added mass, and K_H is the hydrodynamic stiffness. This gives a resulting value of $B_{PTO,opt} = 2.25 \cdot 10^6 kgs^-2$ and $98.4 \cdot 10^6 kgs^-2$ for the HCWEC and the OSWEC respectively.

H. Comparison criteria

The comparison between the long and short crested irregular waves will be performed in terms of the disturbance coefficient, K_D. The K_D coefficient is defined as the ratio between the numerically calculated local total significant wave height, $H_{s,tot}$, and the target incident significant wave height, $H_{s,I}$, imposed along the linear wave generation boundary. In the MILDwave-NEMOH coupled model, the K_D is obtained in the time domain as:

$$K_D = \frac{H_{s,tot}}{H_{s,I}} = \frac{4 \cdot \sqrt{\sum_t^{\Delta t}(\eta_{I,irreg,t} + \eta_{pert,irreg,t})^2 \cdot \frac{dt}{\Delta t}}}{H_{s,I}}, \quad (14)$$

where $\eta_{I,irreg,t}$ and $\eta_{pert,irreg,t}$ are the free surface elevations for irregular incident and perturbed waves in each time step dt and Δt is the time window over which K_d is computed.

III. RESULTS AND DISCUSSION

I. Disturbance coefficient calculation for long and short crested irregular waves

Results for the K_D for Test Case 1 and 2 are shown in Figure 3. The coupling region in the MILDwave-NEMOH coupled model is masked out using a white solid circle and is not considered for the comparison. For the long crested wave case, Figure 3(a), the total wave field obtained is symmetric over the x-axis showing almost no reflection in front of the WEC, while a "wake effect" is clearly visible in the lee of the WEC(s). Around the x-axis as at distance of (x = 500 m) there is a small asymmetry in the "wake effect" due to the coarse grid resolution used for visualization.

For the short crested wave case, 3(b) the same effect can be seen: there is almost no reflection in front of the coupling region, with a "wake effect" appearing in the lee of the WEC(s) that has a smaller magnitude than the one from long crested irregular waves. Furthermore, in this case it can be see that there is no symmetry around the x-axis. It is not possible to obtain a symmetric wake effect of a WEC(s) in short crested waves using a single sea-state, one simulation.

The methodology employed randomly assigns a wave direction θ for each frequency of the discretized spectra, meaning that the frequencies where the WEC is extracting more energy (close to the resonance period of the device) will not necessarily be close to the θ_{mean} and therefore will be generating an asymmetric diffraction and radiation pattern that is interacting with the incident wave field.

To help understand this behaviour in short crested waves results for η of the incident, perturbed and total wave field for Test Cases 7 and 8 are shown in Figures 4 and 5 respectively at the simulation time $t = 100$ s.

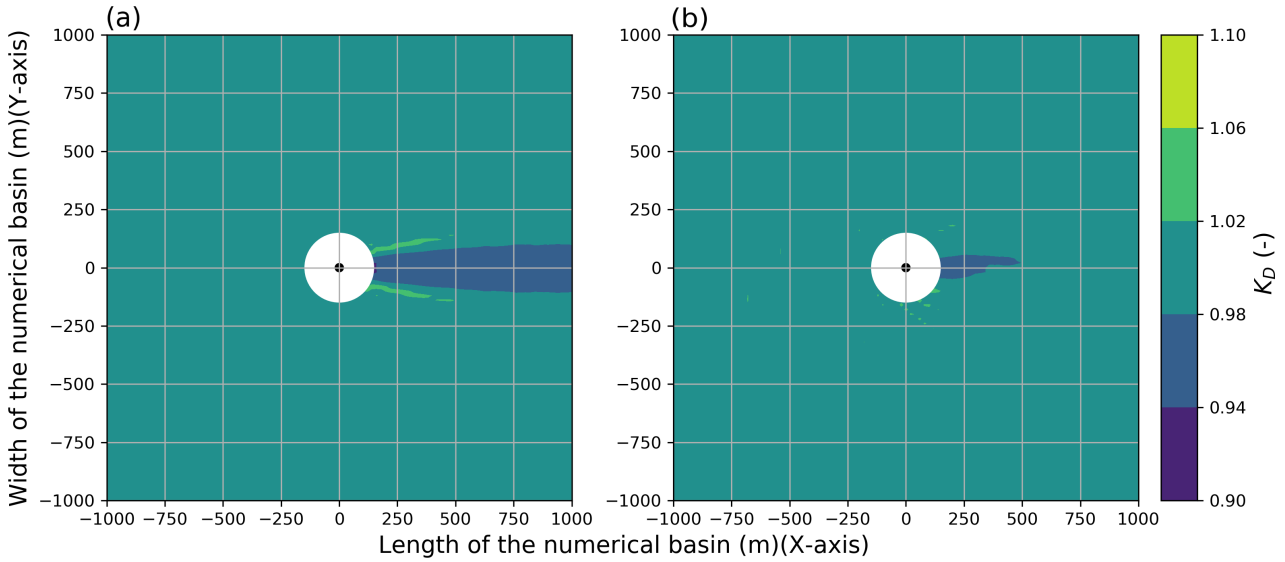

Fig. 3. K_D results for an irregular wave with Tp = 8.0 s and Hs = 2.0 m obtained using the MILDwave-NEMOH coupled model: (a) Test Case 1 ($s_1 = 0$) and (b) Test Case 2 ($s_1 = 15.8$) of Table I. Contour levels are set at an interval of 0.02 of Kd value (-). The coupling region is masked out using a white solid circle which includes the HCWEC (indicated by using black solid circles). Incident waves are generated from the left to the right. S1 indicates the location of cross-sections.

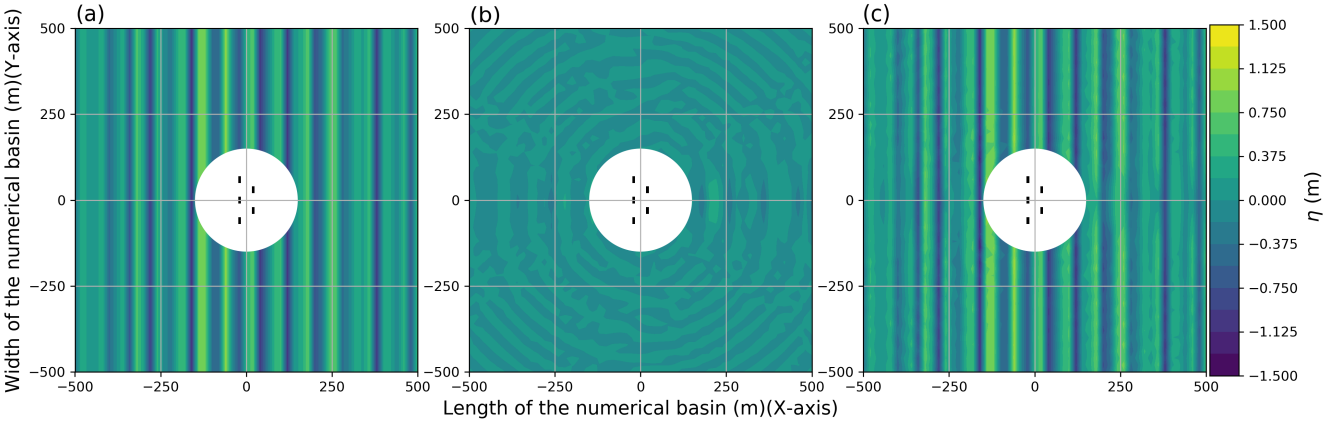

Fig. 4. η (m) results for an irregular wave with Tp = 8.0 s, Hs = 2.0 m and $s_1 = 0$ obtained using the MILDwave-NEMOH coupled model for Test 7: (a) Incident Wave Field, (b) Perturbed Wave Field and (c) Total Wave Field. Contour levels are set at an interval of 0.375 of η value (m). The coupling region is masked out using a white solid circle which includes the 5 OSWECs (indicated by using black solid rectangles). Incident waves are generated from the left to the right.

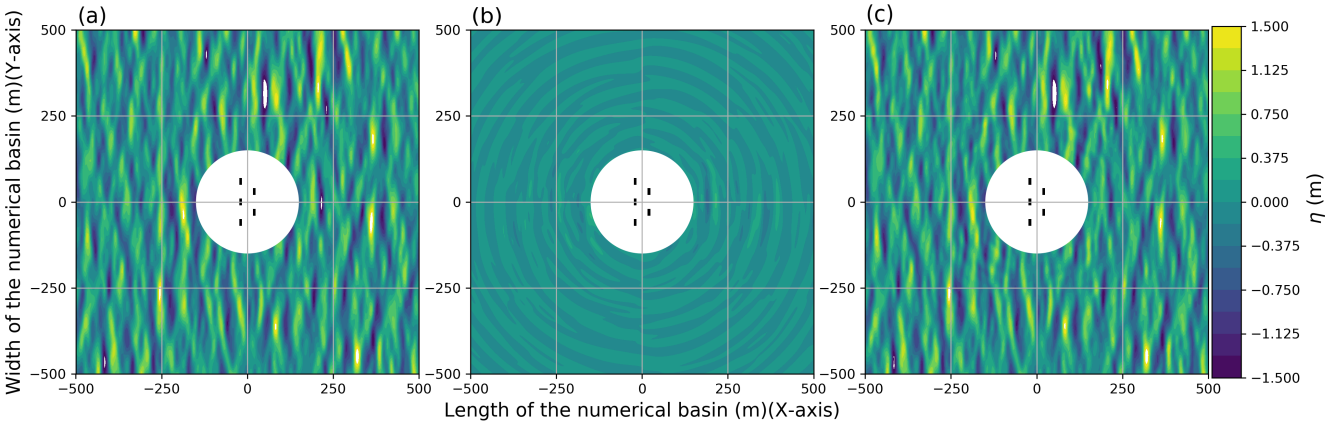

Fig. 5. η (m) results for an irregular wave with Tp = 8.0 s, Hs = 2.0 m and $s_1 = 15.8$ obtained using the MILDwave-NEMOH coupled model for Test 7: (a) Incident Wave Field, (b) Perturbed Wave Field and (c) Total Wave Field. Contour levels are set at an interval of 0.375 of η value (m). The coupling region is masked out using a white solid circle which includes the 5 OSWECs (indicated by using black solid rectangles). Incident waves are generated from the left to the right.

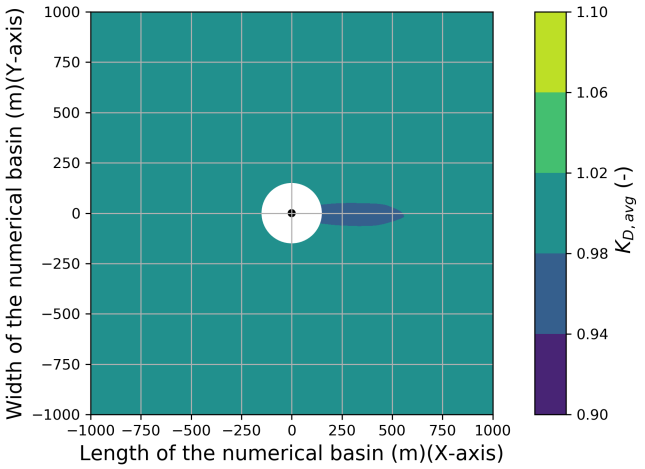

Fig. 6. K_D result, averaged for a total of M = 10 sea states, for an irregular wave with Tp = 8.0 s and Hs = 2.0 m obtained using the MILDwave-NEMOH coupled model for Test Case 2 ($s_1 = 15.8$) of Table I. Contour levels are set at an interval of 0.02 of Kd value (-). The coupling region is masked out using a white solid circle which includes the HCWECs (indicated by using black solid circles). Incident waves are generated from the left to the right. S1 indicates the location of cross-sections.

Test Cases 7 and 8 have been chosen as the 5 OSWEC array

will have the biggest impact in the incident wave field and therefore modifications of the surface elevation around the WEC array are more visible. The coupling region in the MILDwave-NEMOH coupled model is masked out using a white solid circle.

For the long crested waves (Figure 4(c)) it is possible to see the effect of the OSWEC WEC array in η in front and in lee of the coupling region. However, for the short crested waves (Figure 5(c)) the effect of the WEC array in η is smaller and it is only possible to distinguish a small reduction in η in the lee of the WEC array close to the coupling region.

Looking at Figures 4B and 5B we can see a difference in the perturbed surface elevations. In the case of long crested waves the perturbed wave pattern is symmetric according to the x-axis, which is not the case for short-crested waves with the propagating direction changing in each time step.

Therefore for comparing the effect on the total wave field of short crested irregular waves to those of long crested waves it is not possible to use a single simulation (one sea-state) and then obtain the K_D for short crested waves. An average of the K_D over a different number of simulations should be used instead, to assess the impact of short crested waves. In this way it is possible to account for the different attack angles of the frequencies of the discretized spectra close to the resonance period of the WEC(s), where more energy will be extracted from the waves and that is randomly changed in each simulation.

Figure 6 shows the $K_{D,avg}$ for Test Case 2 in Table I for a total of M = 10 simulations with a randomly generated directional spectra in each case. It can be seen that the average tends to be symmetric over the x-axis corresponding with $\theta_{mean} = 0^o$. It can be observed that in front of the coupling region there is almost no reflection, while the "wake effect" in the lee is smaller than for a single simulation, Figure 3(b). Nevertheless the wake effect is smaller than the one generated by long crested irregular waves.

J. Comparison between long and short crested irregular waves

To understand the difference in the "wake effects" of WEC(s) interacting with irregular long and short crested waves longitudinal, cross-sections drawn through the center of the numerical domain for the different Test Cases included in Table I. Figure 7(a) and 7(b) show the results for a single HCWEC and a 5 HCWEC array, and Figure 7(c) and 7(d) show the results for a single OSWEC and a 5 OSWEC array.

In Figure 7 we can see that the "wake effects" of OSWEC are greater than those of HCWEC for the same wave conditions, as they have a wide absorption bandwidth. Furthermore, for all cases there are bigger impacts for long crested irregular waves than for short crested irregular waves. Lower values of K_D in the lee of the array can be observed, since the waves are coming from multiple directions and thus reducing the "lee side" effect.

First, for the case of 1 WEC the difference in K_D between long crested waves and short crested waves is almost negligible after 1 km, lower than 1%.

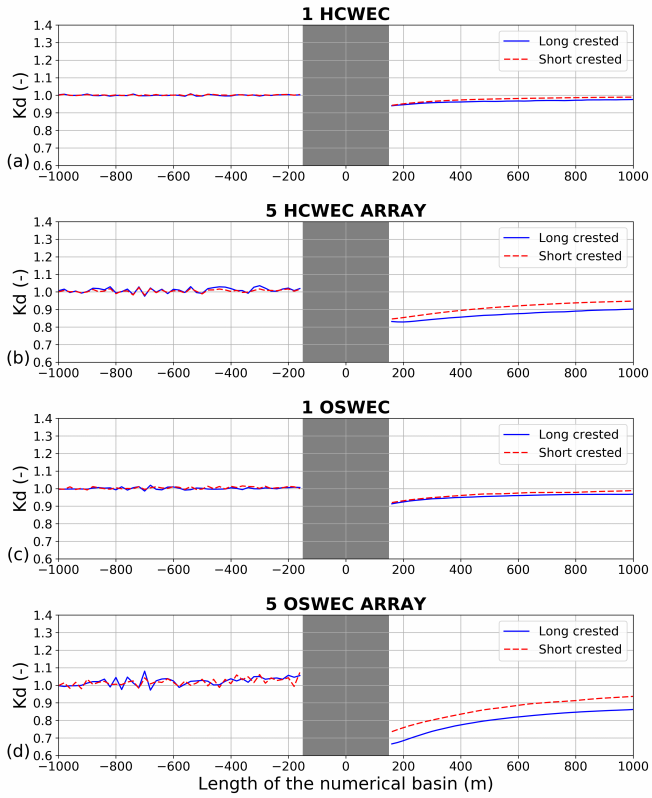

Fig. 7. K_D results for the MILDwave-NEMOH coupled model along one longitudinal cross-sections S1 (left) as indicated in Figure 3 for: (a) Test Casess 1 and 2, (b) Test Cases 3 and 4, (c) Test Cases 5 and 6, and (d) Test Cases 7 and 8. The coupling region is masked out in gray colour and includes the WECs' cross-sections, which are indicated by black vertical areas.

Second, for the case of the 5 WEC arrays there is a K_D difference of 2.4% for the HCWEC and 6.7% for the OSWEC between long crested and short crested irregular waves. This difference in the K_D for irregular and short crested waves is showing that the impact of WEC arrays under short crested waves is less than that of irregular long crested waves.

Thirdly, a trend is noticed when increasing the number of WECs of the array. The difference in K_D between long crested and short crested waves is increased. This observation is also valid when increasing the impact of the WEC modelled, the K_D reduction of OSWEC in the lee of the array is larger than for HCWEC.

IV. Conclusions

In this paper we have shown the difference in the "wake effects" of WECs under the long crested and short crested waves using a coupling methodology between the wave propagation model "MILDwave" and the wave structure interaction solver NEMOH.

First we have demonstrated that it is possible to study the impact of "WEC" arrays under short crested using the aforementioned coupling methodology by averaging a sufficient number of random sea state simulations attacking the WECs. Second, we have shown that the impact of long crested waves is higher than for short crested waves for all Test Cases. It has been shown that the difference in the impact depends on the number of WECs studied and the type of WECs. The difference for 1 WEC simulations for the two objects is almost negligible. When increasing the WECs to a 5 WEC array the impact reduction goes up to 3% for HCWEC and 7% for OSWECs.

We can conclude based on the current results that to avoid over estimating the "wake effects" of WEC arrays it is necessary to study them under short crested waves as the difference in the assessed impact between long and short crested irregular waves can differ substantially when increasing the number of WEC of the array and the WEC type.

References

[1] European Marine Energy Centre (EMEC) Ltd, "Wave Developers Database," Available online: http://www.emec.org.uk/marine-energy/wave-developers/ (accessed on Nov 13, 2018). [Online]. Available: http://www.emec.org.uk/marine-energy/wave-developers/

[2] M. Göteman, C. McNatt, M. Giassi, J. Engström, and J. Isberg, "Arrays of Point-Absorbing Wave Energy Converters in Short-Crested Irregular Waves," *Energies*, vol. 11, no. 4, 2018.

[3] G. Verao Fernandez, V. Stratigaki, and P. Troch, "Irregular wave validation of a coupling methodology for numerical modelling of near and far field effects of wave energy converter arrays," *Energies*, vol. 12, p. 538, 02 2019.

[4] V. Stratigaki, P. Troch, T. Stallard, D. Forehand, J. P. Kofoed, M. al. Folley, M. Benoit, A. Babarit, and J. Kirkegaard, "Wave Basin Experiments with Large Wave Energy Converter Arrays to Study Interactions between the Converters and Effects on Other Users," *Energies*, vol. 7, pp. 701–734, 2014.

[5] G. Verao Fernandez, P. Balitsky, V. Stratigaki, and P. Troch, "Coupling methodology for studying the far field effects of wave energy converter arrays over a varying bathymetry," *Energies*, vol. 11, no. 11, 2018. [Online]. Available: http://dx.doi.org/10.3390/en11112899

[6] P. Troch and V. Stratigaki, "Phase-Resolving Wave Propagation Array Models," in *Numerical Modelling of Wave Energy Converters*, M. Folley, Ed. Elsevier, 2016, ch. 10, pp. 191–216.

[7] V. Stratigaki, P. Troch, and D. Forehand, "A fundamental coupling methodology for modelling near-field and far-field wave effects of floating structures and wave energy devices," *Renewable Energy*, 2019, in press.

[8] A. C. Radder and M. W. Dingemans, "Canonical equations for almost periodic, weakly nonlinear gravity waves," *Wave Motion*, vol. 7, no. 7, pp. 473–485, 1985.

[9] V. Stratigaki, D. Vanneste, P. Troch, S. Gysens, and M. Willems, "Numerical modelling of wave penetration in ostend harbour," in *PROCEEDINGS OF CONFERENCE ON COASTAL ENGINEERING*, J. McKee Smith and P. Lynett, Eds., vol. 32. Engineering Foundation. Council on Wave Research, 2010, p. 15. [Online]. Available: http://dx.doi.org/10.9753/icce.v32.waves.42

[10] C. Beels, P. Troch, G. De Backer, M. Vantorre, and J. De Rouck, "Numerical implementation and sensitivity analysis of a wave energy converter in a time-dependent mild-slope equation model," *Coastal Engineering*, vol. 57, no. 5, pp. 471–492, 2010.

[11] P. Balitsky, G. Verao Fernandez, V. , and P. Troch, "Coupling methodology for modelling the near-field and far-field effects of a Wave Energy Converter," in *Proceedings of the ASME 36th International Conference on Ocean, Offshore and Arctic Engineering (OMAE2017)*, 2017.

[12] T. Verbrugghe, V. Stratigaki, P. Troch, R. Rabussier, and A. Kortenhaus, "A comparison study of a generic coupling methodology for modeling wake effects of wave energy converter arrays," *ENERGIES*, vol. 10, no. 11, 2017.

[13] N. Tomey-Bozo, J. M. A. Babarit, P. Troch, T. Lewis, and G. Thomas, "Wake Effect Assesment of a flap-type wave energy converter farm using a coupling methodology," in *Proceedings of the ASME 36th International Conference on Ocean, Offshore and Arctic Engineering (OMAE2017).*, 2017.

[14] C. Beels, P. Troch, J. P. Kofoed, P. Frigaard, J. V. Kringelum, P. C. Kromann, M. H. Donovan, J. De Rouck, and G. De Backer, "A methodology for production and cost assessment of a farm of wave energy converters," *Renewable Energy*, vol. 36, pp. 3402–3416, 2011.

[15] V. Stratigaki, D. Vanneste, P. Troch, S. Gysens, and M. Willems, "Numerical modeling of wave penetration in ostend harbour," *Coastal Engineering Proceedings*, vol. 1, no. 32, p. 42, 2011. [Online]. Available: https://journals.tdl.org/icce/index.php/icce/article/view/1289

[16] M. Brorsen and J. Helm-Petersen, "On the Reflection of Short-Crested Waves in Numerical Models," in *Proc. of the 26th Int'l Conference on Coastal Engineering, Copenhagen*, 1998, pp. 394–407.

[17] C. Lee and K.-D. Suh, "Internal generation of waves for time-dependent mild-slope equations," *Coastal Engineering*, vol. 34, pp. 35–57, 07 1998.

[18] S. E. Sand and A. E. Mynett, "Directional wave generation and analysis," in *Proceedings of the IAHR Seminar on Wave Analysis and Generation in Laboratory Basins, Lausanne, Switzerland*, 09 1987, pp. 363–376.

[19] P. Vasarmidis, V. Stratigaki, and P. Troch, "Accurate and fast generation of irregular short crested waves by using periodic boundaries in a mild-slope wave model," *Energies*, vol. 12, no. 5, 2019. [Online]. Available: http://www.mdpi.com/1996-1073/12/5/785

[20] A. Babarit and G. Delhommeau, "Theoretical and numerical aspects of the open source BEM solver {NEMOH}," in *Proc. of the 11th European Wave and Tidal Energy Conference 6-11th Sept 2015, Nantes, France*, 2015.

[21] M. Alves, "Wave Energy Converter modelling techniques based on linear hydrodynamic theory," in *Numerical Modelling of Wave Energy Converters*, M. Folley, Ed. Elsevier, 2016, ch. 1, pp. 11–65.

[22] M. Penalba, I. Touzón, J. Lopez-Mendia, and V. Nava, "A numerical study on the hydrodynamic impact of device slenderness and array size in wave energy farms in realistic wave climates," *Ocean Engineering*, vol. 142, no. Supplement C, pp. 224–232, 2017.

[23] M. Penalba, T. Kelly, and J. Ringwood, "Using nemoh for modelling wave energy converters: A comparative study with wamit," in *Proceedings of the 12th European Wave and Tidal Energy Conference(EWTEC 2017)*, 08 2017.

[24] P. Frigaard, J. Helm-Petersen, G. Klopman, C. Standsberg, M. Benoit, M. Briggs, M. Miles, J. Santas, H. Schäffer, and P. Hawkes, "Iahr list of sea parameters: an update for multidirectional waves," in *Proceedings of the 27th IAHR Congress, San Francisco, 10-15 August 1997*, Mansard, Etienne (ed.), Ed. Canada: Canadian Government Publishing, 1997, pDF for print: 11 pp.

[25] V. Stratigaki, P. Troch, T. Stallard, D. Forehand, M. Folley, J. P. Kofoed, M. Benoit, A. Babarit, M. Vantorre, and J. Kirkegaard,

"Sea-state modification and heaving float interaction factors from physical modelling of arrays of wave energy converters," *Journal of Renewable and Sustainable Energy*, vol. 7, no. 7, 2015.

[26] G. Iglesias and R. Carballo, "Wave farm impact: The role of farm-to-coast distance," *Renewable Energy*, vol. 69, pp. 375–385, 2014. [Online]. Available: http://www.sciencedirect.com/science/article/pii/S0960148114002341

[27] J. Abanades, D. Greaves, and G. Iglesias, "Wave farm impact on the beach profile: A case study," *Coastal Engineering*, vol. 86, pp. 36–44, 2014. [Online]. Available: http://www.sciencedirect.com/science/article/pii/S0378383914000179

[28] C. J Cargo, A. Plummer, A. Hillis, and M. Schlotter, "Determination of optimal parameters for a hydraulic power take-off unit of a wave energy converter in regular waves," *Proceedings of the Institution of Mechanical Engineers, Part A: Journal of Power and Energy*, vol. 226, pp. 98–111, 02 2012.